

Paleomagnetic Investigation of Leyte and Biliran Island,  
Central Philippines

by

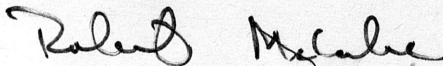
Tiffany A. Ohnstad

College of Geosciences  
Department of Geophysics

Submitted in Partial Fulfillment of the Requirements of the  
University Undergraduate Fellows Program

1985-86

Approved by:



Dr. Robert McCabe

April 1986

## Table of Contents

	Page
List of Tables.....	i
List of Figures.....	ii
Abstract.....	1
Introduction.....	1
Regional Tectonics.....	1
Local Tectonics.....	4
Geology	
Biliran Island.....	7
Central Leyte.....	11
South Central Leyte.....	13
Structural Geology.....	14
Rock Magnetization.....	15
Collection and Laboratory Techniques.....	16
Conclusion.....	34
Acknowledgements.....	34
References.....	35
Appendix.....	36

Note: Format taken from Journal of Geophysical Research

List of Tables

	Page
Table 1 Magnetization and Normlized Magnetization of the Samples.....	24
Table 2 Raw Data.....	27
Table 3 Processed Data at 600 Oersted.....	32

## List of Figures

Page

Figure 1	
Tectonic Map of Study Area.....	2
Figure 2	
Terrane Map of Central Philippines.....	4
Figure 3	
Schematic Time Sequence of Island Arc-Trench Complex....	5
Figure 4	
Paleomagnetic Data, Early-Middle Miocene.....	6
Figure 5	
Beck Model.....	8
Figure 6	
Luyendyk Model.....	9
Figure 7	
Regional Structural Map of Leyte.....	17
Figure 8	
Regional Structural Map of Biliran.....	18
Figure 9	
Location, Access & Coverage Map, Burauen Prospect.....	19
Figure 10	
Normalized Magnetism vs. Demagnetizing Field Strength.	21
Figure 11	
Vector Diagram of Sample JL-9.....	23
Figure 12	
Stereographic Projection, 600 Oersted Demagnetization.	26

## ABSTRACT

Six sample sites were chosen from over 20 sites located on Biliran and Leyte islands in the central Philippines to determine whether or not rotations associated with either a collision between the Palawan continental terrane and the Philippine Archipelago or fault movement along the Philippine Fault had occurred. Sample analysis using a normalized sample magnetization as a function of demagnetizing field strength graph and a Zijderfeld diagram indicated that the samples were demagnetizing properly. Older sites, JL-71 and JB-37 showed clockwise rotation associated with an island arc collision, while younger samples, JB-17, JB-3, and possibly JL-26 indicated counterclockwise rotation in agreement with fault-related rotations.

## INTRODUCTION

The paleomagnetic investigation of the Philippine Islands of Leyte and Biliran was designed to achieve two goals: first, to attempt to identify whether or not any rotation of the sites had occurred in the past, and secondly to attempt to identify those rotations with either clockwise rotations associated with the tectonic movement of the Philippine Island arc, or counterclockwise rotations associated with predicted rotations for left-lateral faults such as the 1200 KM long Philippine Fault of the study area. If counter-clockwise rotations were observed in the fault region, an attempt would be made to explain these rotations by comparing the geologic setting to one of two models which are subsequently reviewed.

## REGIONAL TECTONICS

The tectonic history of the Philippine Island arc presented by geologic evidence is complex and may have included collisions with another arc, reversals of subduction zones and the superposition of young arcs over older, inactive ones (McCabe, et

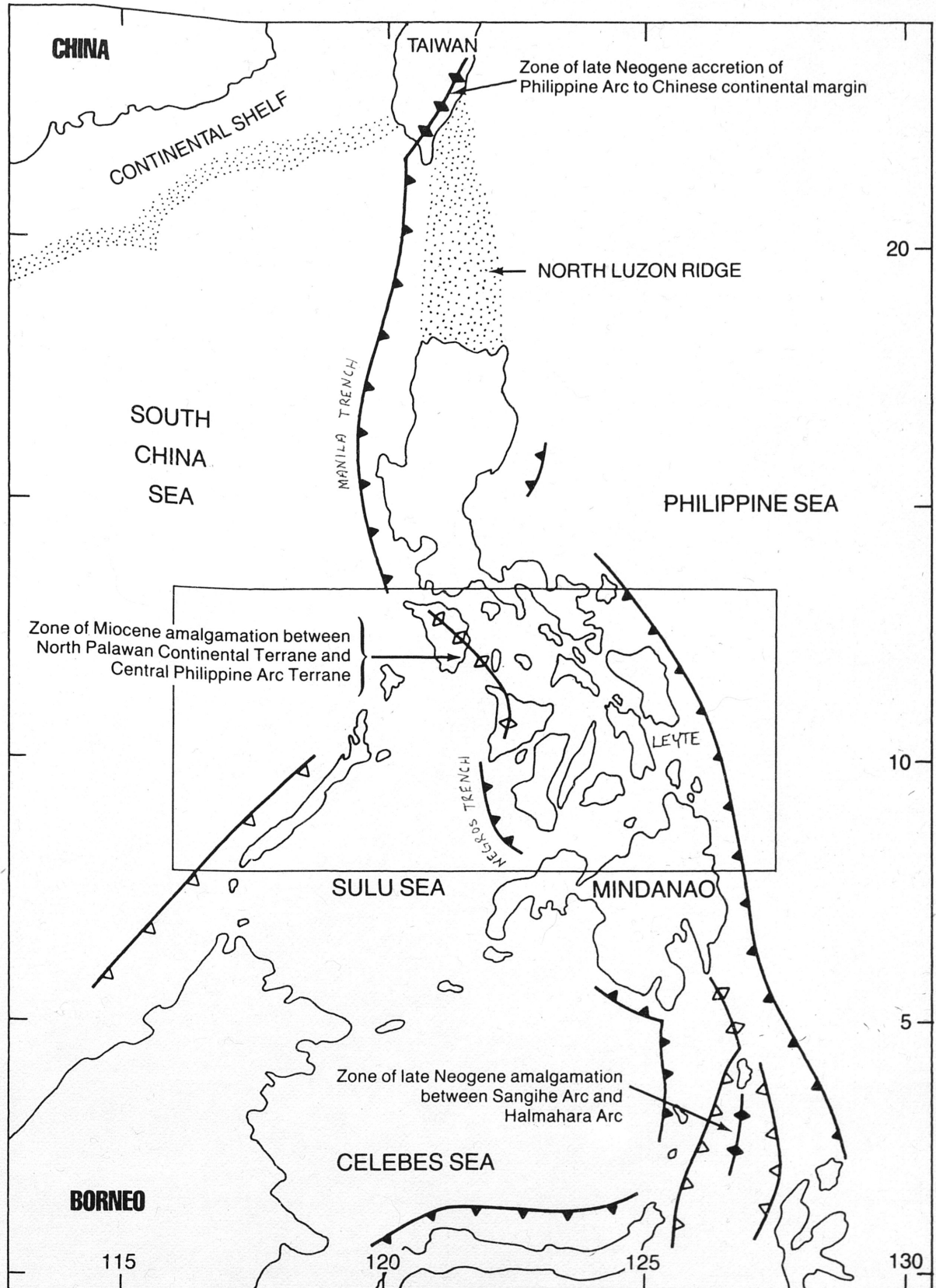


**Figure 1**—Simplified tectonic map of the western margin of the Philippine Sea Plate. Shown are zones of Neogene amalgamation in central Philippines and Molucca Sea. Also shown is zone of accretion of Philippines to Asian continental margin. Insert shows location of Figure 2. Single-sided hash marks represent zones of subduction, hash marks on upper plate. Diamonds show zones of collisions; solid ones are Pliocene to Recent collisions and open ones are Miocene in age. (Aquino, et.al., 1983)

al.,1982). Presently, the Manila Trench to the north and the Negros Trench to the south are active subduction zones (Figure 1). Between the two trenches, the metamorphic continental terrane of Palawan does not appear to be undergoing subduction (Figure 2). This is expected since the continental material of the Palawan block is too bouyant to be subducted. One model proposed by McCabe, et al.(1982) predicts the development of thrusts and folds followed by clockwise rotation of material south of the continental block and counterclockwise rotation north of the block because the continental block cannot undergo subduction (Figure 3).

Geologic and structural evidence suggest such a collision between the Philippine Island arc and the Palawan Continental terrane. On the island of Panay, the eastern half of the island is composed of two tectonic provinces, both of which show evidence of volcanism and volcanic-derived sediments associated with an island arc. A melange containing blocks of peridotite, gabbro, serpentine matrix composes the Antique Range (Figure 2) along the western coast of the island (McCabe, et al., 1982). West of the mountains is a series of thrust faults which runs north to northwest which places red chert, peridotite and metabasalt over limestone and tuffaceous sediments. In the northwest corner of the island, a valley which runs north-south, and is possibly fault controlled, separates the Buruanga Peninsula composed of quartz, feldspathic schist, and marble which have been intruded by a biotite-quartz diorite pluton from the Antique Range. The composition of these rocks is strong evidence that the peninsula is continent derived and related to the Palawan block. Paleomagnetic data shown in Figure 4, also substantiate the rotations predicted by the collisional model.

## LOCAL TECTONICS

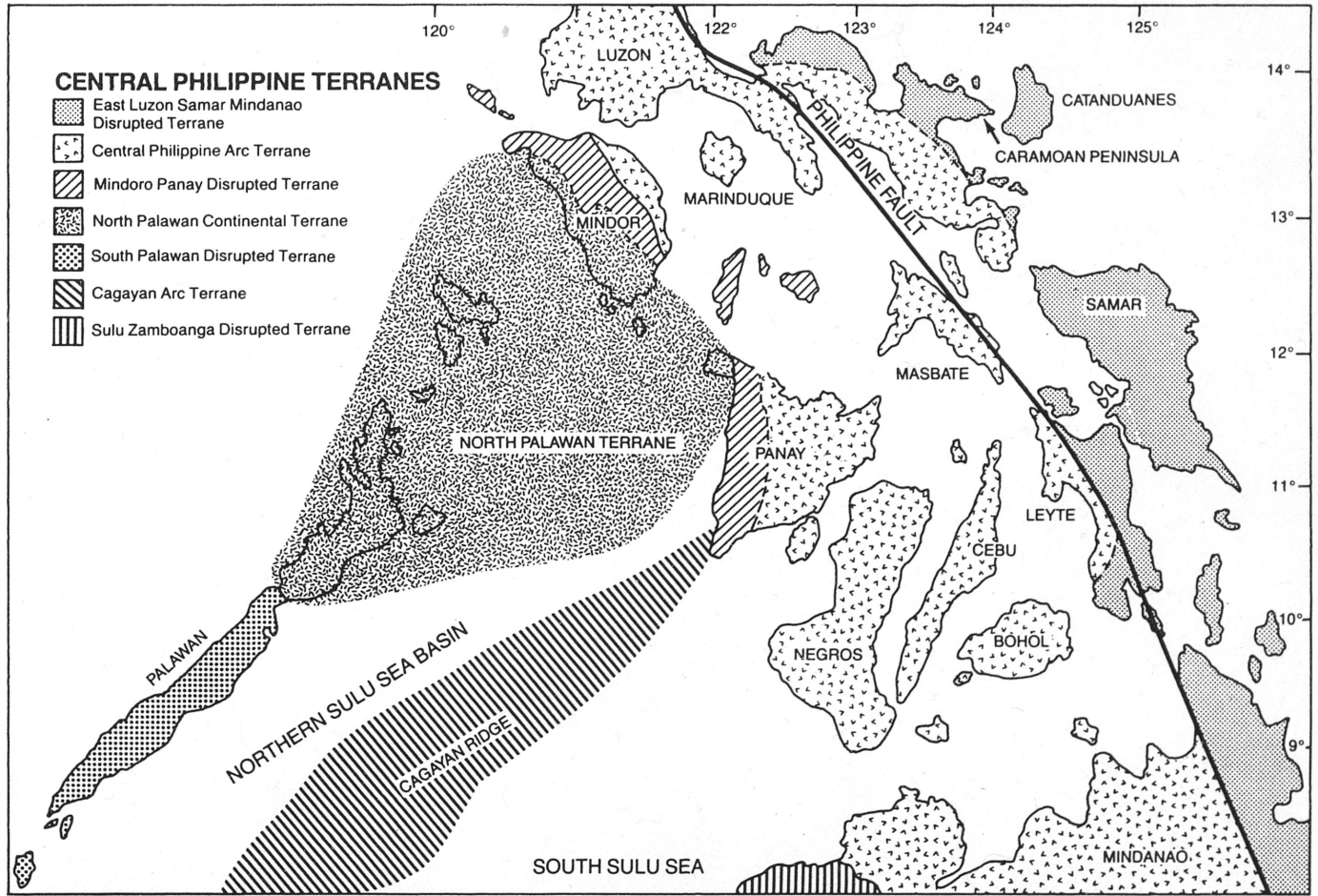


**Figure 2**—Terrane map of central Philippines as described in text. Terrane boundaries are only to be regarded as approximate. Boundary of CPAT and ELSDMT is shown with respect to westward occurrence of ophiolites. No displacement is shown on Philippine Fault. Although it is likely that this fault offsets CPAT with respect to ELSDMT, lack of data in region makes it impossible to predict the amount of this offset. (McCabe, et.al., 1985)



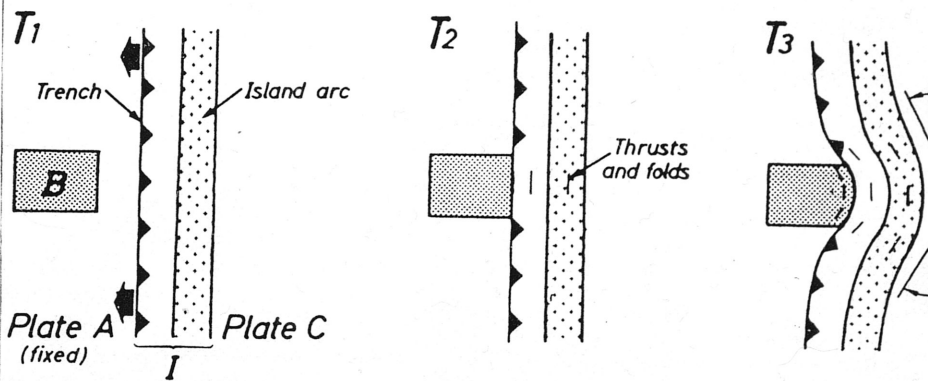


Figure 3. Schematic time sequence of island arc-trench complex I (located on the western margin of plate C), approaching nonsubductable continental fragment B on oceanic plate A. Plate A is assumed stationary. At  $T_2$ , trench I collides with B. After collision, B locally arrests westward migration of plate C. This results in compressional forces that are directed normal to line of intersection of B and plate C (collision zone). This compression results in development of fold and thrust belts on both fragment B and adjacent area of plate C. Segments of I north and south of collision zone will continue to migrate to left. This migration will result in tectonic rotations shown at  $T_3$ .

(McCabe, et.al., 1982)

# EARLY-MIDDLE MIOCENE

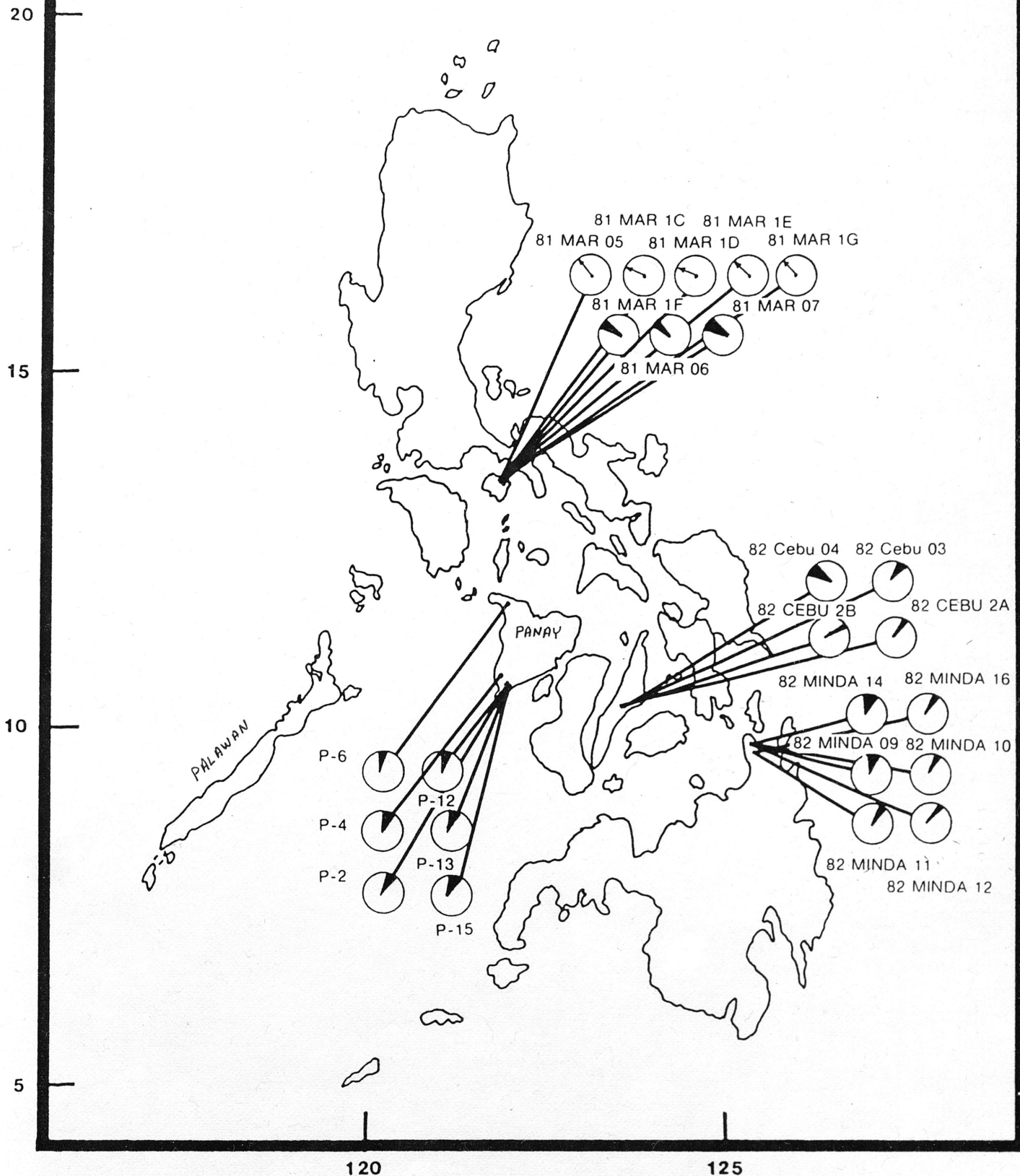


Figure 4

In addition to the rotations predicted by collisional tectonics, two models have been developed to explain rotations which have been observed in strike-slip fault regimes. The first model was proposed by Myrl E. Beck, Jr. (1976) to explain motion of crustal blocks within a zone of distributed shear. In California the shear between the North American and Pacific plates is distributed over a region which is defined by the San Andreas Fault and its related fault system of subparallel, branching, and en-echelon right lateral faults. Rigid blocks of crust trapped within the shear zone would be translated and rotated in a ball bearing-like fashion (Figure 5). The rotation would be clockwise in the case of a right lateral system and counter-clockwise for a left lateral system.

The second model was proposed by Bruce Luyendyk, et al. (1980). In this model, in addition to the right lateral fault system of subparallel faults, conjugate sinistral faults associated with the shear couple are also present (Figure 6). As movement occurs along the dextral faults, rotation of the blocks bounded by left lateral faults occurs. As the model demonstrates, not only is clockwise motion predicted, but left slip occurs simultaneously as well.

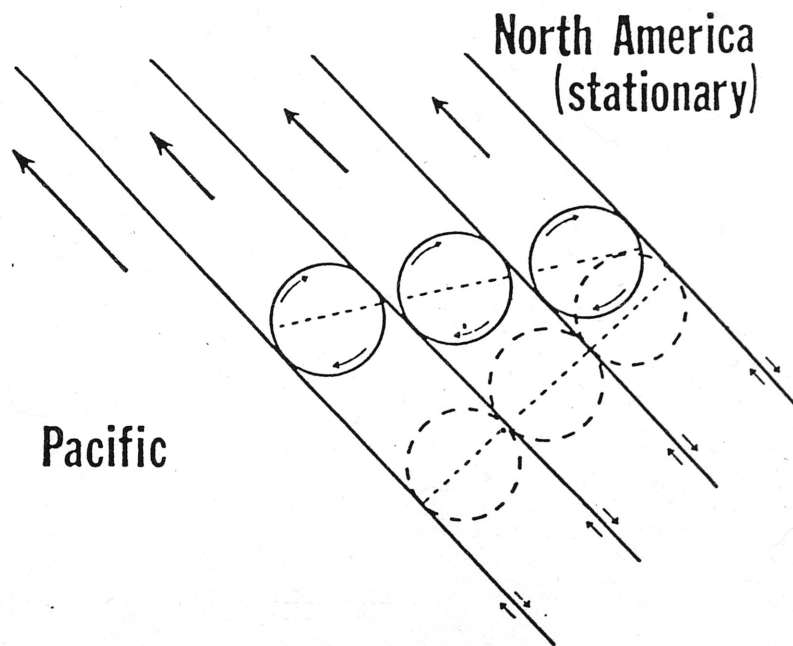
## **GEOLOGY**

### **Biliran Island<sup>1</sup>**

The Catmon Pyroxene Andesite which outcrops on the southwestern side of the island contains two members. The lower member is a fine-grained pyroxene andesite containing hornblende, and the upper member is a porphyritic pyroxene andesite.

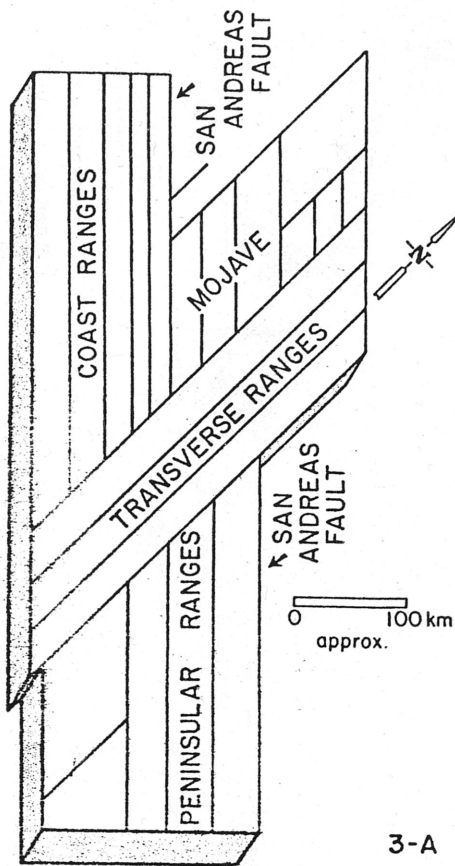
The Naliwatan Andesite which composes Mt. Naliwatan in north-central Biliran is a series of andesite flows of fine-grained, light-gray pyroxene andesite with minor

<sup>1</sup>  
Espiritu, 1980.

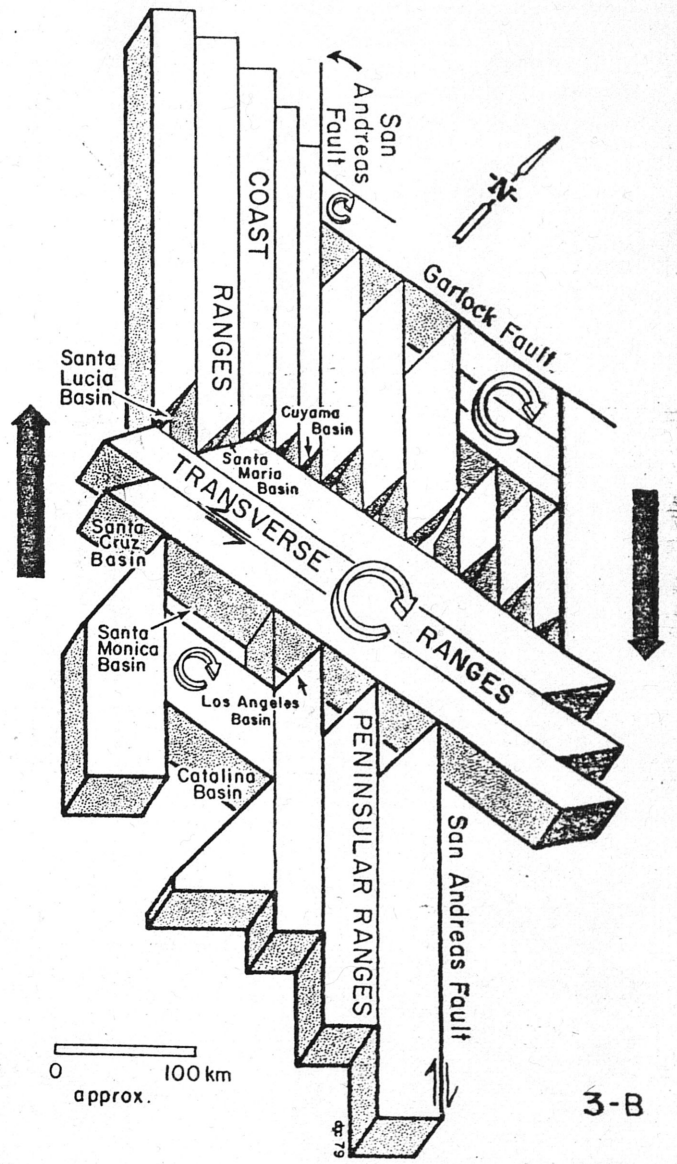


Beck Model

Figure 5: An idealized model showing northwestward translation and clockwise rotation of rigid crustal blocks in a northwest-trending right-lateral shear zone along the westernmost Cordillera within North America. Heavy diagonal lines represent faults within a zone of distributed shear. Crustal blocks (represented by circles) can rotate ball-bearing fashion or move northwestward without rotation (After Beck, 1976).



3-A



3-B

Figure 6 A rotation model for southern California tectonic history. Faults used in the model are: Coast Ranges west from San Andreas = Cuyama, Rinconada, Nacimiento, Hosgri, and Santa Lucia Bank. Peninsula Ranges-west from San Andreas = San Jacinto, Elsinore, Newport-Inglewood, and East Santa Cruz-San Clemente. Transverse Ranges = Big Pine-Pinto Mountain, Santa Ynez-Blue Cut, Simi(?) -Hayfield, and Malibu Coast-Santa Monica-Salton Creek. In the Mojave region, the rotated block is bounded by the Garlock, Calico, and Manix-Cady faults. A. Inferred initial fracture pattern and prerotation geometry for Oligocene time in southern California. B. Miocene-Pliocene time (?) geometry after the clockwise rotation event which probably occurred in mainly Miocene time. Sinistral and dextral slip has occurred and detrital basins have opened at the joins of the rotated

and unrotated blocks. C. Late Miocene time geometry showing the through-cutting of the Transverse Ranges by San Andreas, San Gabriel, and Elsinore faults, and the jump of the San Andreas fault east to the San Jacinto. Basins are shown filled. D. Present geometry showing offset of the Transverse Ranges along the San Andreas fault. Miocene basins are not shown here.

Luyendyk Model

amounts of hornblende and biotite. The groundmass is composed of laths of fine-grained, massive, sodic plagioclase.

The Kandako Basalt is a group of flows which range from dark gray pyroxene andesite to hypocrySTALLINE porphyritic augite basalt. They are found around Mt. Kandako (Mt. Gumansan) in the center of Biliran. The basalt displays sub-ophitic texture, and thin section reveals calcic plagioclase, augite, magnetite, olivine, and glass.

The Biliran Volcanics include lava flows and pyroclastic materials which make up the composite Biliran Volcano (Mt. Suiro). The basalt which is present is a hypocrySTALLINE, pilotaxitic, porphyritic pyroxene basalt containing plagioclase, augites, hypersthene, hornblende, magnetite, and glass. Also present is a dark gray porphyritic pyroxene andesite with euhedral pyroxene crystals in a plagioclase matrix. There is a light gray hornblende andesite containing phenocrysts of hornblende. Finally, the agglomerates are composed of boulders of basalt and andesite in a vesicular andesite lava matrix.

The Panamao Volcanics which constitute Mount Panamao in the corner of the island contain a propylitic hornblende andesite, a flow-banded, fine-grained pyroxene andesite/tuff, and a tuffaceous sandstone. The hornblende andesite flow, exposed on the southern side of Mt. Panamao, is gray with conspicuous euhedral laths of hornblende in a medium matrix of sodic plagioclase. The pyroxene andesite is light gray and aphanitic with vesicular and flow-banded structure present. It is exposed north of Mt. Panamao near Kawayan. The tuffaceous sandstone is an unsorted, dark brown sandstone containing pebble to boulder size andesite clasts. Graded bedding and laminae indicate a marine volcanic deposit.

The Asluman Volcanics are a porphyritic, dark colored pyroxene andesite (basaltic andesite) characterized by cubic-shaped pyroxene in a fine-grained matrix.

Found in dome-shaped Mount Sayao, the Sayao Hornblende Dacite is composed of dacite and andesite flows containing large hornblende crystals embedded in a coarse-grained matrix. Both the dacite and the andesite are porphyritic, but the dacite may be distinguished from the andesite by its lighter gray color and coarser texture.

The Villa Vicenta Limestone outcrops west of Villa Vicenta Hot Springs in the east-central portion of the island. It is a hard but porous, buff-colored, reefal limestone containing andesite pebbles.

### Central Leyte<sup>2</sup>

Geologic data were limited for the island of Leyte and so the stratigraphy presented here, taken from central Leyte, should be considered representative of the entire island.

The Leyte Ultramafic Complex, a group of moderate to highly serpentinized ultramafics contains members of highly brecciated masses cut by intricate calcite, dolomite, and occasional quartz. Minerals present include augite, enstatite, labradorite, chlorite, magnetite, and calcite.

The Burauen Volcanics consist of three members. The first is an andesite porphyry, notably altered as indicated by chloritization and pyritization. Silicification and argillization are common along fracture planes and the intercalating pyroclasts. Epidote was observed in veinlets with disseminated pyrite. The second member is a pyroxene andesite which sometimes grades into basaltic andesite. It contains ortho and clinopyroxenes, plagioclases, magnetite, and apatite. The final member is an oxy-hornblende andesite with vesicular structure. The Albuera Diorite was originally

<sup>2</sup>  
Aquino, 1983.

misnamed, for it is actually not a diorite but a pyroxene-bearing hornblende andesite in the area near the Palanas River. A plutonic body NNE of Albuera town is also known by this name. It is a biotite-bearing hornblende andesite which also contains plagioclases, quartz, calcite, some magnetite, and veinlets of epidote.

The Leyte Central Formation is a sequence of deposits containing volcanic breccia agglomerates, tuff breccia, and pyroclastics with local intrusions and intercalations of pyroxene andesites.

The Albuera Formation is composed of marine clastics, tuffaceous sandstone, reefal limestone, and minor beds of conglomerates.

Dacitic pyroclasts with abundant inclusions of reworked hornblende dacite pumice compose the Daguitan Tuff. Detrital subordinate fragments of dacite and andesite were also observed.

The Burauren Pyroclastic Deposits are distinct volcanic ejecta composed of andesite tephra, tuff breccia, lahars, volcanic sandstone, and tuff agglomerate.

Lava which does not flow, but rather forms cylindrical or cumulo-form barriers in the craters of volcanoes or causes doming of the rocks above them have been named plug domes. They are composed of biotite-bearing pyroxene to hornblende andesite and contain such minerals as plagioclase, magnetite, hornblende, pyroxene, and biotite.

The Lobi Volcanics located near Mt. Lobi and Majunag are hornblende andesite tuff breccias and pyroclasts of pyroxene-hornblende andesite.



The Mahagnao Volcanics consist of a hornblende-rich andesite and a hornblende dacite. The andesite is medium-grained with small quantities of pyroxene. The dacite is medium-to coarse-grained with a porphyritic texture.

### South Central Leyte<sup>3</sup>

The Bito Ultramafics found in Lake Bito and the Calanipawan area are highly brecciated and fractured, but texturally massive. They are serpentinized with abundant flakey minerals.

The Calanipawan Limestone is corraline in origin with interstitial micrite and bioclasts.

The Marabong Volcanic Complex contains two members. The lower member contains basaltic andesite breccia, agglomerates with tuffaceous lava cement, and a basaltic andesite lava flow. The basaltic andesite grades into breccia with clasts and cement of the same composition. This is overlain by a massive, dark gray to black (sometimes reddish due to secondary hematite) basaltic andesite lava flow and agglomerates with tuffaceous to andesitic cement. Crystals of subhedral to euhedral hornblende and pyroxene can be found. The upper member is a pyroxene andesite which forms agglomerates and/or breccias and a tuff unit. The pyroxene andesite is lighter than the basaltic andesite and embedded with larger, well formed crystals of pyroxene. It is an amygdaloidal, porphyritic, pyroxene andesite with orthophric texture in a matrix of magnetite specks, ferromagnesian, and abundant feldspar.

The Bato Volcanic Complex has three members: the Talisayan Volcanics, the Parasanon Sedimentary deposits, and the Bato Andesite. Within the Talisayan Volcanics are a hornblende andesite flow, and flow breccia and agglomerates intercalated

<sup>3</sup>  
Bayrante, 1981.

with tuff. The hornblende andesite is silicic and often grades into the flow breccia. It has phenocrysts of angular and fragmented plagioclase and green hornblende in a feldspathic, glass-bearing matrix. Overlying the andesite are agglomerates intercalated with a vitreous, friable, and dacitic tuff. The agglomerates have cobble-to-boulder-sized clasts of hornblende andesite in a tuffaceous cement.

### STRUCTURAL GEOLOGY

Six NE trending strike-slip faults have been located in the field on Biliran Island and are identified in Figure 8. They are the Volcan, Kalambis, Anas, Tenego, Bool, and Culaba faults. A ridge offset along the strike of the Anas indicates right lateral movement. It is the only one of the six in which the direction of movement is known positively.

On Leyte, the Cagbana Fault runs at N 35 W intersecting Marabong River to the northwest, traversing southeastwards along aligned ridges west of Mt. Calarabayan. Fracture readings serve as the only evidence of postulated left-lateral fault movement. East of Cagbana Fault about 3.5-4.0 KM is the San Antonio Fault whose trace is characterized by the alignment of domes and ridges. Offsetting of the Balere and Kamambanan rivers suggests sinistral movement also. These structures are possibly branches of the sinistral Philippine Fault which cuts the entire length of Leyte and extends some 1200 KM overall. Field observations show that this fault may have as much as 150 KM of offset (Robert McCabe, per.com.). A regional compressive stress striking WNW was brought about by the subduction of the Philippine Sea

Plate along the Philippine Trench east of the southern islands and along the Manila Trench bordering the northern islands to the west.

## ROCK MAGNETIZATION

The results of my work are based upon the measurement of magnetization of minerals such as magnetite, which compose a small percentage (usually  $< 5\%$ ) of the total composition of a rock. A brief description of rock magnetization will enable a better understanding of the contents of this presentation.

Magnetization is associated with the orbital motion of electrons in an atom. The electron travelling about the nucleus is equivalent to a current loop; thus, it has a corresponding magnetic moment known as the orbital magnetic moment. Because an electron also spins about its axis, it has a spin magnetic moment. The total dipole moment of an atom is the resultant sum of the orbital and spin magnetic moments which may or may not sum to zero. When atoms or molecules are placed in an external magnetic field, the dipole moments of the atoms tend to align themselves parallel or anti-parallel to the external field depending upon whether the net moment was non-zero or zero, respectively. For most atoms, this magnetization, called induced magnetization, disappears after the external field is removed. The atoms of interest to paleomagnetic study are those which retain a magnetization after the field is removed. This is known as remnant magnetization and can be destroyed if the substance is heated above a critical temperature called the Curie temperature. At the Curie temperature, random thermal agitation of the atoms destroys the alignment of the dipoles. The remnant magnetization can also be removed by applying an external field in the direction opposite the original magnetizing field. The strength of this

field, the coercivity or coercive force, is directly proportional to the strength of the remnant magnetization.

## COLLECTION AND LABORATORY TECHNIQUES

There were 147 samples from over 20 sites in our study area on the islands of Leyte and Biliran in the central Philippines collected during the summer of 1985. Oriented samples were obtained either by portable drill or as handsamples which were drilled later in the laboratory. For the purposes of my research, six sample sites were chosen, three on Biliran Island and three on Leyte. The first site, JB-37, is located along the southeastern coast of Biliran Island east of Cabucgayan (Fig. 7 and Fig. 8). Sites JB-3 and JB-17 are located within 2 KM of one another. JB-3 is situated along the northwest coast of Biliran, approximately 2 KM northeast of Kawayan, and JB-17 is 2 KM northeast of JB-3 or 4 KM northeast of Kawayan (Fig. 7 and Fig. 8). On the island of Leyte itself, JL-26 lies on the northeast coast, 1 KM NW of Santo Nino in the Biliran Strait area (Fig. 7 and Fig. 9). JL-71 is located in the Carigara Bay area of Leyte, 2 KM SE of Pinamopoan. The final site, JL-9, is situated directly within the Philippine Fault zone in north central Leyte near the Tongonan geothermal plant (Fig. 7 and Fig. 9).

The vector components of the magnetization of each sample were measured with a cryogenic magnetometer at the University of Houston. The sample is inserted between pickup coils producing a DC persistent current which is sent to the detector. In this case, the detector is the Superconducting Quantum Interference Device (SQUID). Since the sample does not have to be rotated as in a spinner magnetometer, the three components of magnetization can be measured at one time. The SQUID in essence is

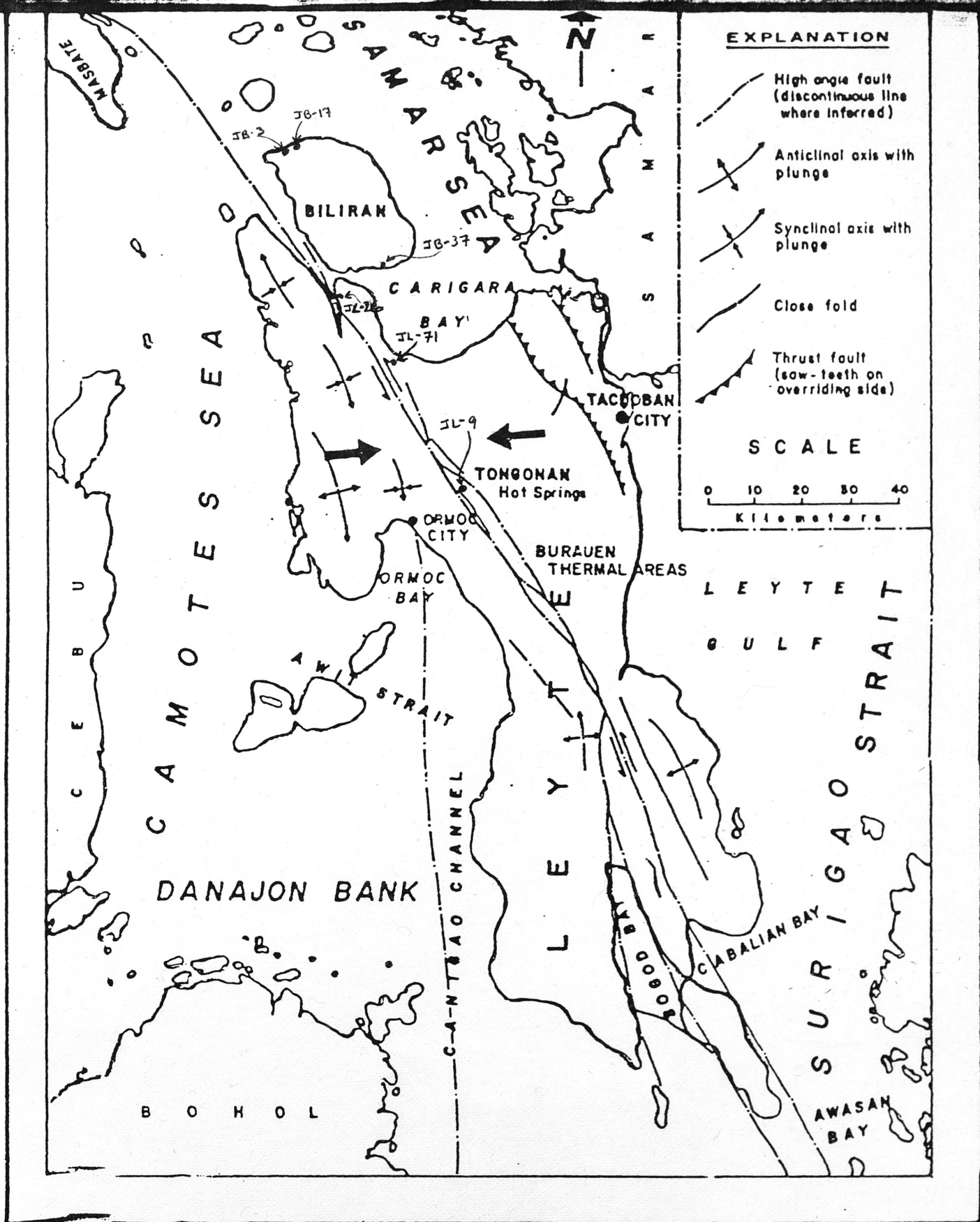


**FIG. 7 REGIONAL STRUCTURAL MAP OF LEYTE**

(After Geologic Map of the Phils., Bureau of Mines and Geos., 1962)

(Bayrante, 1981)

FAULT  
 INFERRED FAULT  
 LARGE ALTERED GROUND  
 STEAMING VENTS

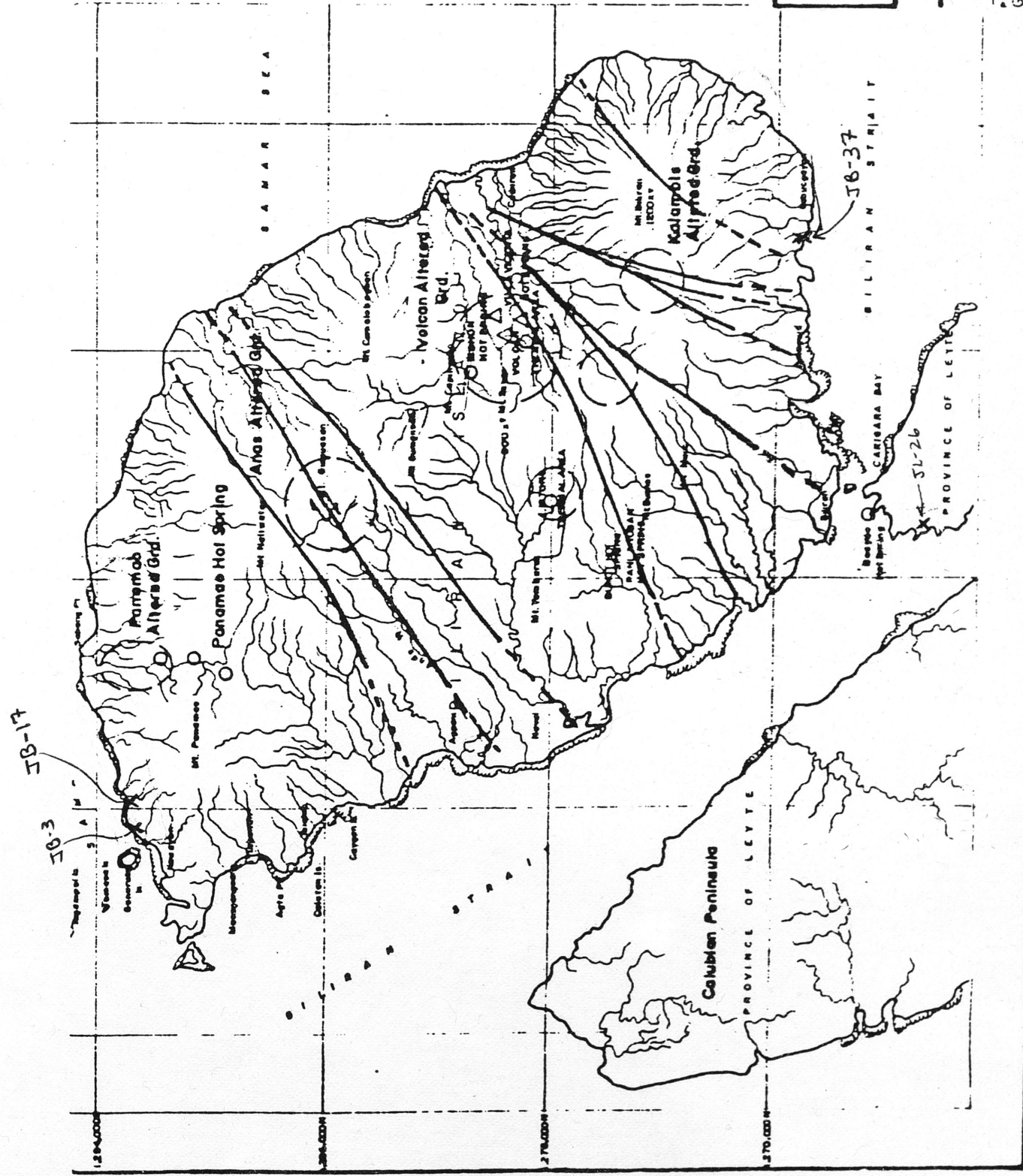
BILIRAN GEOTHERMAL PROSPECT  
 BILIRAN ISLAND  
 MAP SHOWING STRUCTURES AND  
 THERMAL MANIFESTATION

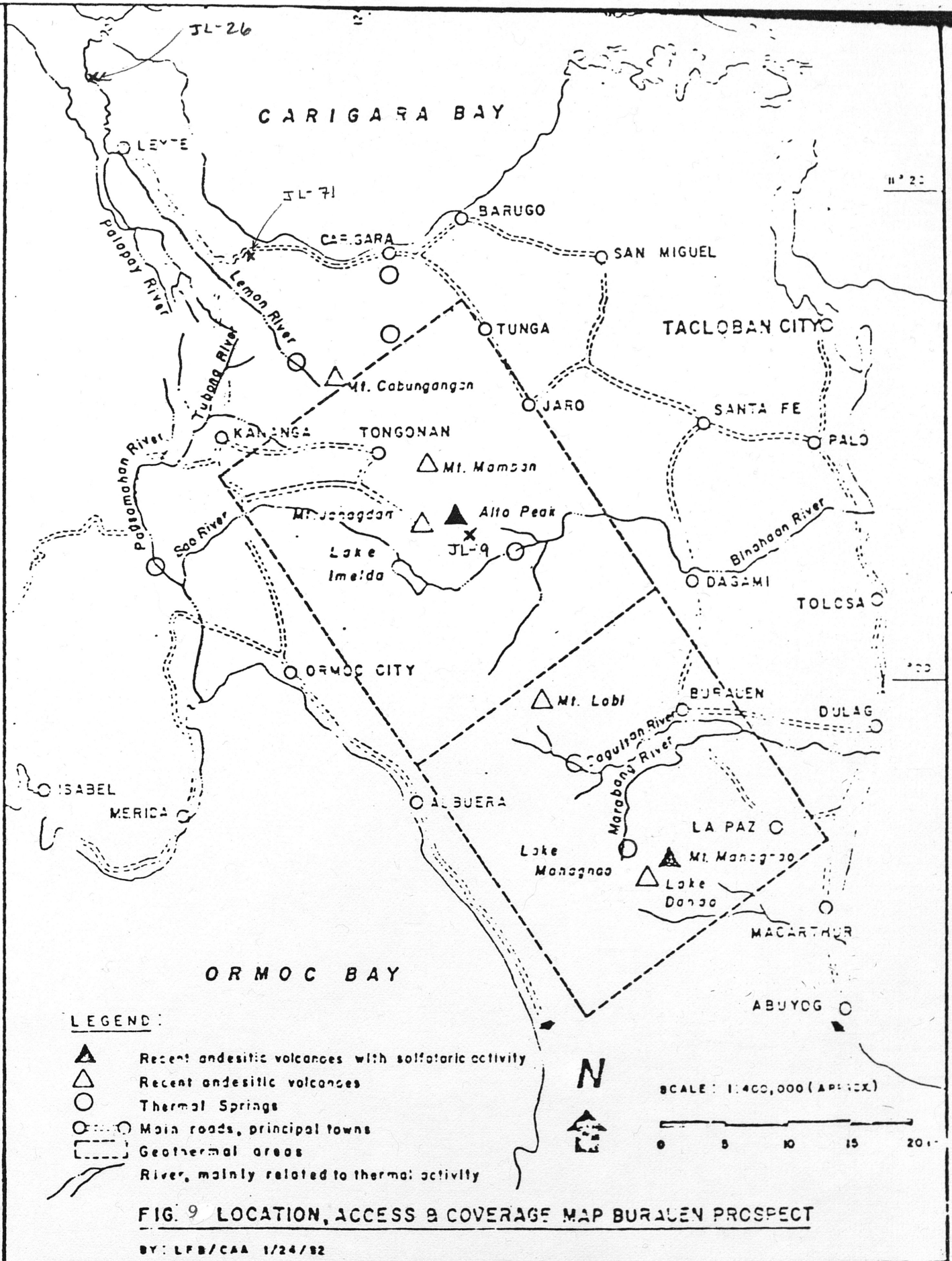
Figure 8

Scale: 1:50,000

PHOENIX ENERGY DEVELOPMENT CORPORATION  
 GEOTHERMAL DIVISION  
 HEADQUARTERS: 1000 BOWEN DRIVE, BOSTON, MASSACHUSETTS

(Espiritu, 1980)





(Bayrante, 1981)

a superconducting ring with a constriction. The change in the magnetic field of the sample causes a current to flow in the superconducting ring. The current is measured and used to obtain the magnetization of the sample.

In order to isolate the stable components of magnetization (i.e. those with a high coercive force) acquired as each sample cooled in the presence of the earth's magnetic field from secondary magnetizations, the alternating field (AF) technique of demagnetization was used. The AF technique is designed to randomize the lower coercivity components the sample may have obtained from exposure to secondary fields and remagnetization which may have occurred as ground water altered magnetite to hematite.

After the magnetization which the sample had in the field, the natural remnant magnetization, has been measured, the sample is placed in an exponentially decaying alternating field usually generated by a solenoid. In order to expose all directions of the sample's magnetization to the peak demagnetizing field, the specimen is tumbled about two perpendicular axes which are mutually perpendicular to the axis of the demagnetizing coil. Components of magnetization with a coercivity,  $H_c = H \cos O$  (where  $H$  is the peak value of the alternating field and  $O$  is the angle between  $H$  and the relevant component of magnetization) will be randomly oriented. The magnetization is remeasured. Then the maximum value of the demagnetizing field is increased and the sample is again placed within the field. This procedure was performed for peak values of 50, 100, 150, 200, 300, 400, and 600 Oe for my samples.

Figure 10 shows a normalized graph of the ratio of the magnetization after each demagnetization to the initial natural remnant magnetization as a function of maximum field intensity. The negative slope of each of the samples after 100 Oe indicates



Normalized Magnetism vs.  
Demagnetizing Field Strength

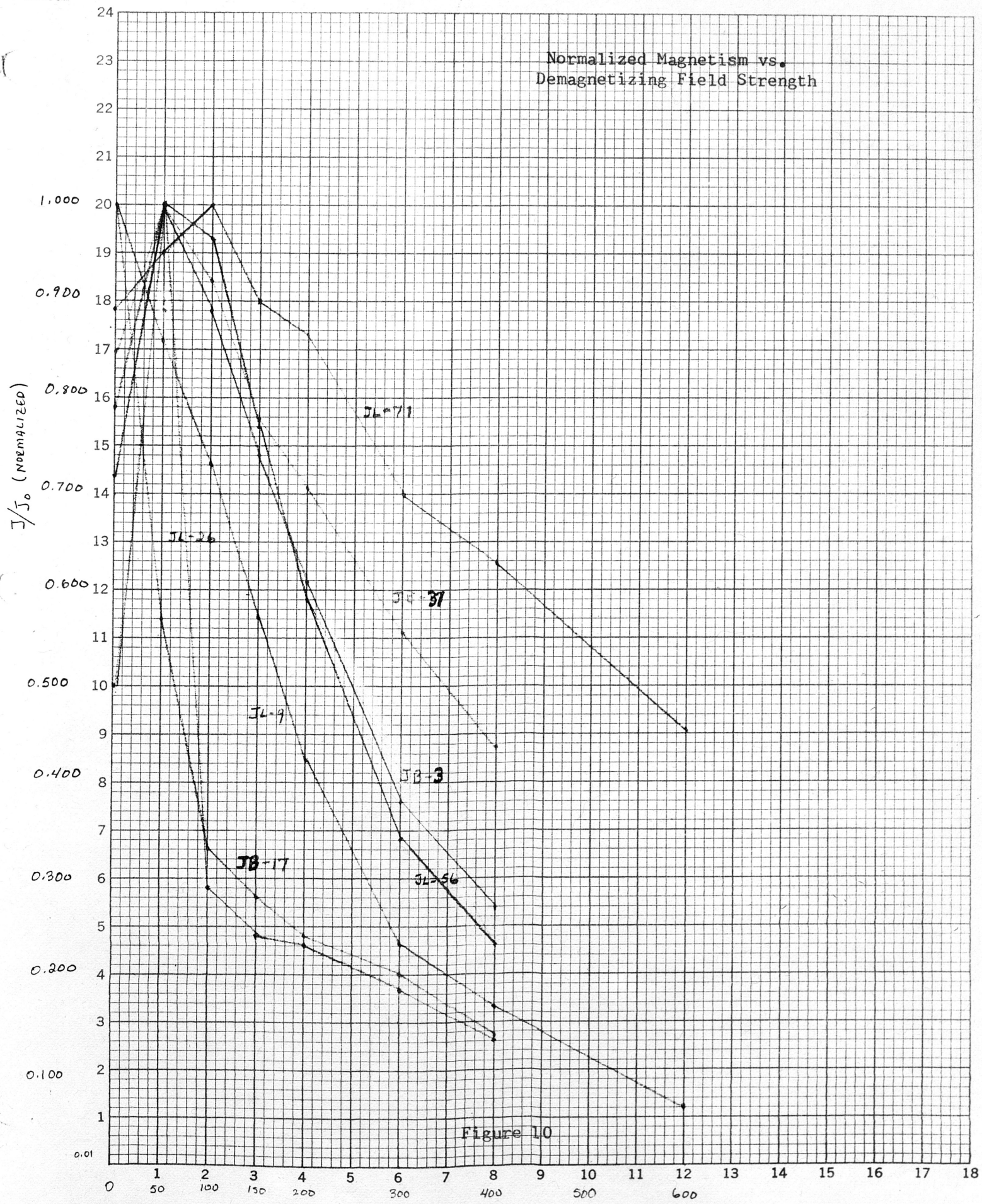


Figure 10

that the lower coercive force components of magnetization are being properly removed. Samples JL-71 and JB-37, which have higher final values of normalized  $J/J_0$ , contain hematite as the magnetic carrier.

In addition to the graph of  $J/J_0$  as a function of peak demagnetization field strength, a vector or Zijderfeld diagram (Figure 11) was used to determine whether or not the magnetization being measured in each sample is a stable component. For each step in the demagnetization process, the angle of declination was calculated as follows:

$$\frac{\cos^{-1}(X)}{\sqrt{(X^2 + Y^2)}}$$

where X and Y are the X and Y components of the sample's magnetic field vector. This angle measured from the X-axis determines the direction on my diagram. The magnitude of the vector was obtained by setting  $J/J_0$  at the natural remnant magnetization equal to two inches on my graph. The angle of inclination given by:

$$\sin^{-1}(Z/J)$$

where Z is the Z component of the sample's magnetization and J is the magnitude of the magnetization (Table 1), determines the angle of inclination on my diagram. The magnitude is identical to that given above for the declination.

To interpret the Zijerfeld diagram, the behavior of vector values for demagnetizing values of greater than 200 Oe must be examined. Each time the value of the demagnetizing field is increased, a greater amount of the magnetization of the sample is removed. If the component of magnetization lies in a single direction, the vector diagram will show an approximate straight line of decay toward the origin. This uni-directional component being removed is the characteristic component of magnetization of the sample and is assumed to be the primary component of magnetization

W, up

VECTOR DIAGRAM  
OF  
SAMPLE JL-9

X - DECLINATION  
O - INCLINATION

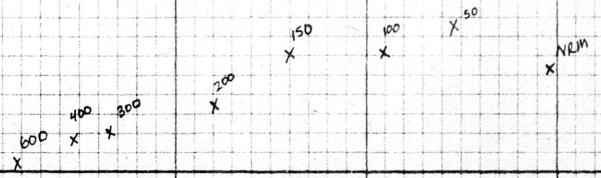


Figure 11

MEAD PRODUCTS, DAYTON, OHIO 45463

SAMPLE	$J_0$	J(50)	J(100)	J(150)	J(200)			
JL-26	0.0908	0.1810	0.05286	0.04417	0.04205			
JB-37	0.05002	0.05886	0.05424	0.04574	0.04150			
JL-9	0.1797	0.1544	0.1315	0.1030	0.07631			
JB-17	0.01410	0.008012	0.004673	0.003985	0.003428			
JL-56	0.01616	0.02248	0.02171	0.01739	0.01329			
JL-71	0.02855	0.03045	0.03195	0.02912	0.02771			
JB-3	0.05417	0.06858	0.06115	0.05095	0.04168			
	J(300)	J(400)	J(600)					
JL-26	0.03365	0.02391	—					
JB-37	0.03275	0.02575	—					
JL-9	0.04134	0.02962	0.01079					
JB-17	0.002833	0.002087	—					
JL-56	0.007647	0.005255	—					
JL-71	0.02247	0.02013	0.01452					
JB-3	0.02607	0.01846	—					
	$\frac{J_0}{J_0}$	$\frac{J(50)}{J_0}$	$\frac{J(100)}{J_0}$	$\frac{J(150)}{J_0}$	$\frac{J(200)}{J_0}$	$\frac{J(300)}{J_0}$	$\frac{J(400)}{J_0}$	$\frac{J(600)}{J_0}$
JL-26	1.00	1.9934	0.5822	0.4865	0.4631	0.3706	0.2633	—
JB-37	1.00	1.1767	1.0844	0.9144	0.8297	0.6547	0.5148	—
JL-9	1.00	0.8592	0.7318	0.5732	0.4247	0.2301	0.1648	0.0600
JB-17	1.00	0.5682	0.3314	0.2826	0.2431	0.2009	0.1480	— .1154
JL-56	1.00	1.3911	1.3434	1.0761	0.8224	0.4732	0.3252	—
JL-71	1.00	1.0665	1.1191	1.0110	0.9706	0.7870	0.7051	0.5086
JB-3	1.00	1.2660	1.1289	0.9406	0.7694	0.4813	0.3408	—
	$\frac{J_0}{J_0(N)}$	$\frac{J(50)}{J_0(N)}$	$\frac{J(100)}{J_0(N)}$	$\frac{J(150)}{J_0(N)}$	$\frac{J(200)}{J_0(N)}$	$\frac{J(300)}{J_0(N)}$	$\frac{J(400)}{J_0(N)}$	$\frac{J(600)}{J_0(N)}$
JL-26	0.5017	1.000	0.2921	0.2441	0.2323	0.1859	0.1321	—
JB-37	0.8498	1.000	0.9216	0.7771	0.7051	0.5564	0.4375	—
JL-9	1.000	0.8592	0.7318	0.5732	0.4247	0.2301	0.1648	0.0600
JB-17	1.000	0.5682	0.3314	0.2826	0.2431	0.2009	0.1480	—
JL-56	0.7189	1.000	0.9657	0.7736	0.5912	0.3402	0.2338	—
JL-71	0.8936	0.9530	1.000	0.9034	0.8673	0.7032	0.6301	0.4545
JB-3	0.7899	1.000	0.8917	0.7430	0.6077	0.3802	0.2692	—

Table 1. Magnetization and Normalized Magnetization of the Samples

that the sample acquired when it cooled in the presence of the earth's magnetic field. This may be assumed for two reasons: 1) The geology from which the sample was taken was examined and no evidence that the sample was reheated above the Curie temperature resulting in a reorientation of the sample's magnetic field as it cooled in a new external field was found. 2) Since the magnetization of a sample is approximately 1000 times stronger than the earth's magnetic field, the sample will not be remagnetized by the earth's field, if it is assumed that the earth's field did not suddenly increase intensity by 1000 times its normal intensity. Figure 11 shows excellent straight line decay above 200 Oe.

For each sample number shown on the raw data (Table 2), the two numbers in the first column represent two measurements of the magnitude of magnetization in the X direction. The second column represents the same for the Y direction, and the third for the Z direction. The third number in each of the columns represents the error between the two measurements. The number on the far right represents the error in total magnitude between the two measurements. Errors of less than 0.025 were larger than this value, the sample was remeasured.

The X, Y, and Z directions given in the raw data are only reference directions and do not necessarily correspond to the actual north, east, and vertical directions in the field. A computer program called Magfile was used to perform a vector transformation on the raw data. The inclination and declination of the drill core, its weight, and the inclination and declination of any desired bedding corrections were input into the program to produce the sample inclination and declination.

The values of inclination and declination from the 600 Oe demagnetization (Table 3) for the sites were plotted on a stereographic projection (Figure 12). Sites JL-26, JB-17, JB-3, and JL-71 which clustered about 180 degrees were magnetized when

LEYTE (600)

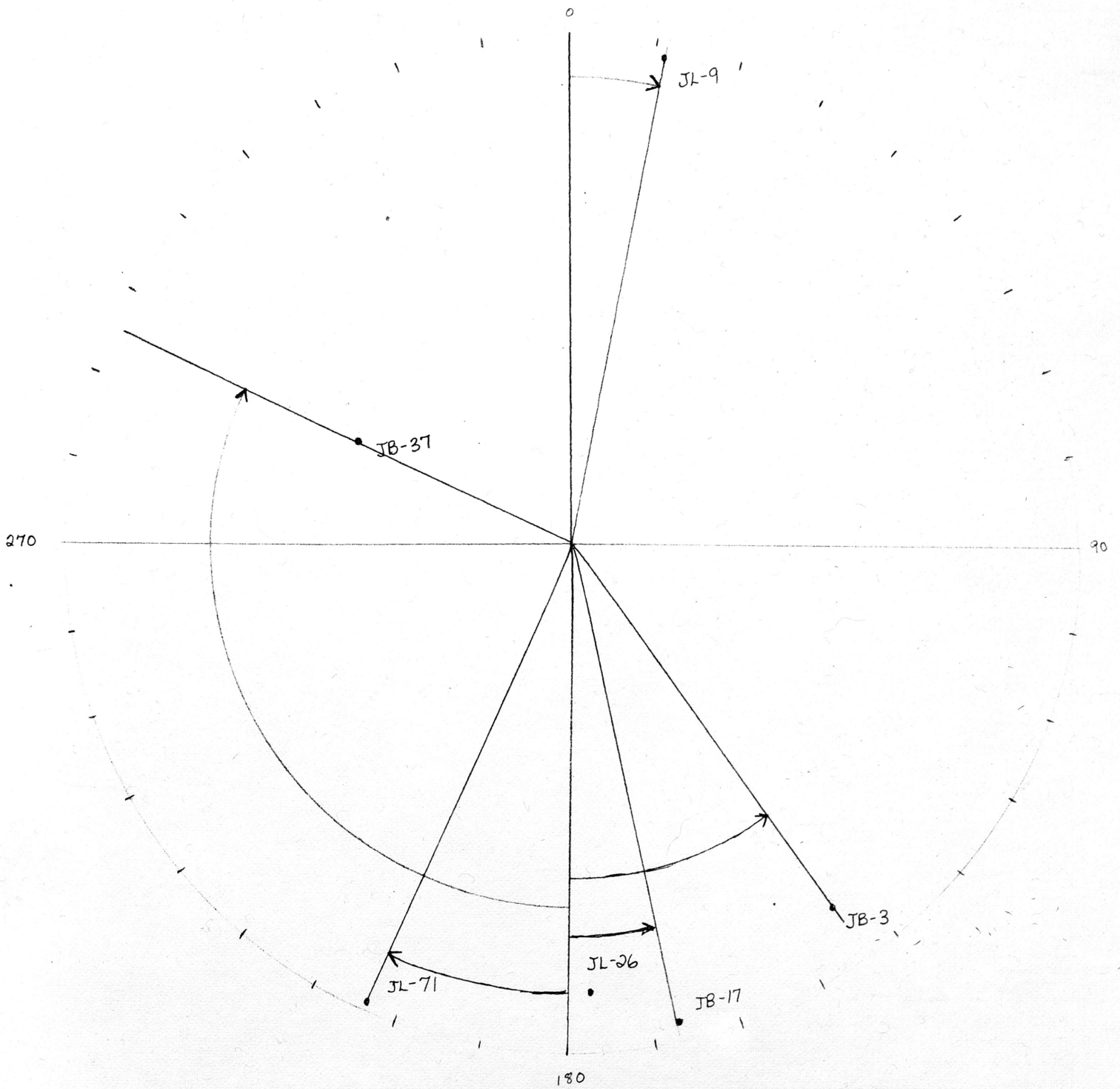


Figure 12. Stereographic Projection, 600 Oersted Demagnetization

LEYTE-NRM

SAMPLE NO. JL-9			
0.12724	-0.0218	0.12499	
0.1266	-0.02307	0.12544	
6.39999984E-04	1.27E-03	4.5000008E-04	8.30090665-03
SAMPLE NO. JB-17			
-0.01306	5.18E-03	1E-03	
-0.01306	5.24E-03	9.9E-04	
0	6.00000021E-05	9.99999975E-06	4.31523478E-03
SAMPLE NO. JL-26			
-0.07842	-7.27E-03	-0.04517	
-0.07831	-6.41E-03	-0.04553	
1.10000023E-04	8.6E-04	3.59999962E-04	0.0103390399
SAMPLE NO. JB-3			
0.02555	0.041	0.02432	
0.0258	0.04075	0.02487	
2.4999999E-04	2.50000012E-04	5.50000012E-04	0.0120690337
SAMPLE NO. JL-71			
0.01192	0.02569	-3.95E-03	
0.01212	0.02554	-3.7E-03	
1.99999995E-04	1.50000007E-04	2.49999999E-04	0.0123826177
SAMPLE NO. JB-37			
-0.01163	0.04585	0.01633	
-0.01125	0.04574	0.01677	
3.79999994E-04	1.09999979E-04	4.39999996E-04	0.0118292178

LEYTE-DEMAG(50)

SAMPLE NO. JB-37			
0.02963	0.04432	0.02527	
0.02865	0.04424	0.02589	
9.79999997E-04	8.00000126E-05	6.20000013E-04	0.0197496177
SAMPLE NO. JB-3			
0.01834	0.06595	-4.31E-03	
0.01899	0.06579	-3.63E-03	
6.50000009E-04	1.60000054E-04	6.8E-04	0.0139140158

Table 2. Raw Data

SAMPLE NO. JL-26			
-0.04278	0.02336	-0.02953	
-0.04258	0.02344	-0.02953	
1.99999951E-04	8.00000053E-05	0	3.78362814E-03

SAMPLE NO. JL-9			
0.10538	-0.03204	0.10831	
0.1046	-0.03335	0.10843	
7.79999973E-04	1.30999999E-03	1.19999982E-04	9.90580696E-03

SAMPLE NO. JB-17			
-7.26E-03	2.01E-03	2.76E-03	
-7.23E-03	2.09E-03	2.72E-03	
3.00000029E-05	7.99999998E-05	4.00000008E-05	0.0117740824

SAMPLE NO. JL-71			
0.01431	0.02678	-2.58E-03	
0.01457	0.02662	-2.29E-03	
2.60000001E-04	1.60000003E-04	2.90000001E-04	0.138272735

LEYTE-DEMAG(100)

SAMPLE NO. JB-37			
0.02851	0.0406	0.02183	
0.0288	0.04026	0.02225	
2.90000004E-04	3.39999997E-04	4.20000004E-04	0.011307602

SAMPLE NO. JL-26			
-0.03958	0.02029	-0.02854	
-0.03935	0.02071	-0.02859	
2.29999991E-04	4.19999997E-04	4.99999878E-05	9.10892607E-03

SAMPLE NO. JL-9			
0.0914100001	-0.02668	0.09084	
0.09074	-0.02795	0.09092	
6.70000009E-04	1.27000001E-03	7.9999998E-05	0.0109338719

SAMPLE NO. JB-3			
0.01502	0.05891	-6.81E-03	
0.01561	0.05878	-6.11E-03	
5.89999992E-04	1.30000015E-04	6.99999997E-04	0.0151218338

SAMPLE NO. JB-17			
-2.62E-03	-5.3E-04	3.81E-03	
-2.66E-03	-5.1E-04	3.83E-03	
3.9999999E-05	1.99999997E-05	2.00000004E-05	0.0104846726

SAMPLE NO. JL-71			
0.01869	0.02588	1.06E-03	
0.01902	0.02564	1.4E-03	
3.3000001E-04	2.40000001E-04	3.4E-04	0.0166254513

Table 2 (cont.)



LEYTE-DEMAG(150)

SAMPLE NO. JB-17

-4E-04	-2.13E-03	3.33E-03	
-4.5E-04	-2.07E-03	3.39E-03	
5.00000001E-05	6.00000003E-05	6.00000021E-05	0.0247148255

SAMPLE NO. JL-26

-0.03449	0.01962	-0.02577	
-0.03437	0.01996	-0.02583	
1.19999982E-04	3.40000006E-04	6.00000058E-05	7.71821313E-03

SAMPLE NO. JB-3

0.01251	0.049	-6.38E-03	
0.01301	0.0489	-5.84E-03	
5.00000002E-04	1.00000019E-04	5.40000001E-04	0.0145760112

SAMPLE NO. JL-9

0.07084	-0.02603	0.07001	
0.07048	-0.02689	0.0701	
3.60000035E-04	8.59999993E-04	9.00000159E-05	9.09719295E-03

SAMPLE NO. JL-71

0.01423	0.02554	2.07E-03	
0.01379	0.02532	2.36E-03	
4.39999996E-04	2.20000009E-04	2.9E-04	0.0196114837

SAMPLE NO. JB-37

0.02689	0.03062	0.02083	
0.02755	0.02942	0.02159	
6.60000013E-04	1.20000001E-03	7.59999988E-04	0.0342441488

LEYTE-DEMAG(200)

SAMPLE NO. JL-26

-0.03067	0.01557	-0.02425	
-0.03042	0.016	-0.02418	
2.50000005E-04	4.29999997E-04	7.00000018E-05	0.0119440737

SAMPLE NO. JB-3

0.01469	0.03865	-5.14E-03	
0.01506	0.03851	-5.28E-03	
3.69999998E-04	1.40000018E-04	1.40000002E-04	0.0100693517

SAMPLE NO. JB-17

0	-2.3E-03	2.58E-03	
0	-2.26E-03	2.54E-03	
0	3.99999999E-05	3.99999999E-05	0.0165013352

Table 2 (cont.)

SAMPLE NO. JB-37			
0.02689	0.02757	0.01554	
0.027	0.0271	0.016	
1.09999986E-04	4.69999999E-04	4.59999996E-04	0.0160685694

SAMPLE NO. JL-71			
0.01627	0.02223	2.62E-03	
0.01651	0.02212	2.92E-03	
2.40000009E-04	1.10000008E-04	3E-04	0.0144198845

SAMPLE NO. JL-9			
0.05276	-0.01438	0.05321	
0.05241	-0.01512	0.05338	
3.49999988E-04	7.4E-04	1.70000028E-04	0.0109562365

LEYTE-DEMAG(300)

SAMPLE NO. JL-9			
0.02868	-8.32E-03	0.02853	
0.02848	-8.92E-03	0.02868	
2.00000001E-04	6E-04	1.5E-04	0.0157215631

SAMPLE NO. JB-17			
5.2E-04	-2.25E-03	1.59E-03	
4.6E-04	-2.3E-03	1.64E-03	
5.99999997E-05	4.99999997E-05	5.00000001E-05	0.032738224

SAMPLE NO. JL-26			
-0.02389	0.0149	-0.01841	
-0.0237	0.01521	-0.01843	
1.89999984E-04	3.09999999E-05	1.99999995E-05	0.010822298

SAMPLE NO. JB-37			
0.02153	0.01984	0.01457	
0.02166	0.0196	0.0149	
1.3E-04	2.40000009E-04	3.30000003E-04	0.0130777455

SAMPLE NO. JB-3			
9.16E-03	0.02407	-3.96E-03	
9.53E-03	0.02401	-3.61E-03	
3.69999998E-04	6.00000058E-05	3.49999998E-04	0.0196724561

SAMPLE NO. JL-71			
0.0125	0.0184	3.11E-03	
0.01261	0.0183	3.39E-03	
1.09999999E-04	1.00000005E-04	2.79999999E-04	0.0141083018

Table 2.(cont.)

LEYTE-DEMAG(400)

SAMPLE NO. JB-37			
0.0167	0.01553	0.01181	
0.01687	0.01531	0.01214	
1.70000007E-04	2.19999998E-04	3.29999992E-04	0.0167595164

SAMPLE NO. JL-71			
9.62E-03	0.01752	2.34E-03	
9.77E-03	0.01743	2.53E-03	
1.5E-04	9.00000014E-05	1.90000002E-04	0.0128284964

SAMPLE NO. JL-9			
0.02231	-7.35E-03	0.01793	
0.02228	-7.65E-03	0.01808	
3.00000029E-05	3E-04	1.5E-04	0.0113679903

SAMPLE NO. JB-17			
4.3E-04	-1.71E-03	1.07E-03	
4.4E-04	-1.79E-03	1.03E-03	
1.00000001E-05	8.00000003E-05	4.00000004E-05	0.0431307567

SAMPLE NO. JL-26			
-0.01745	8.51E-03	-0.01395	
-0.01731	8.76E-03	-0.01399	
1.40000004E-04	2.50000001E-04	3.99999999E-05	0.0120988757

SAMPLE NO. JB-3			
6.04E-03	0.01725	-2.73E-03	
6.32E-03	0.01714	-2.51E-03	
2.8E-04	1.10000008E-04	2.2E-04	0.0201906006

LEYTE-DEMAG(600)

SAMPLE NO. JL-71			
8.16E-03	0.01182	2.06E-03	
8.34E-03	0.0117	2.16E-03	
1.79999999E-04	1.20000004E-04	1E-04	0.0164144487

SAMPLE NO. JL-9			
7.13E-03	-1.68E-03	7.84E-03	
7.22E-03	-1.79E-03	7.91E-03	
9.00000014E-05	1.1E-04	7.00000018E-05	0.0146778294

Table 2 (cont.)

LEYTE-UF(600)

SAMPLE NO.	STRAT POSH	SAMPLE		CORRECTED		INTENSITY (EMU/GM)	ERR	DATE
		DEC	DIP	DEC	DIP			
.85 JL-71(600)		0.0	211.7	-14.2	211.7	-14.2	4.83E-08	.02 325
.85 JL-9(600)		0.0	10.7	-2.3	10.7	-2.3	3.59E-08	.01 325.
.85 JB-17(600)		0.0	167.0	3.3	167.0	3.3	2.16E-07	.01 326
.85 JB-3(600)		0.0	144.4	-10.2	144.4	-10.2	1.36E-06	.01 326.
.85 JL-56(600)		0.0	225.0	71.5	225.0	71.5	3.72E-07	.01 326
.85 JL-26(600)		0.0	177.6	10.7	177.6	10.7	1.93E-06	.01 326
.85 JB-37(600)		0.0	341.6	-8.0	341.6	-8.0	2.15E-06	.01 326

Table 3. Processed Data at 600 Oersted

the earth's magnetic field was the reverse of what it is presently. Also, sample JB-37 is known to be reversely magnetized. Site JL-9 is normally magnetized. Sites JL-71 and JB-37 are known to be older than 20 million years (Robert McCabe, per.com.) from evidence of folding noted in the field. These samples are both rotated clockwise which agrees with the rotation predicted by the collision of the Philippine Island arc with the Palawan continental terrane. Younger sites, JB-17 and JB-3, and possibly JL-26, show counterclockwise rotation which is opposite to the expected rotation. Though JL-26 does show counter-clockwise rotation, the angle of rotation is within the +5 error associated with paleomagnetic measurements. It is now important to remember that all of the sites are located in the right lateral strike-slip regime of the Philippine Fault. If one returns to the model proposed by Luyendyk, clockwise rotation and left-lateral offset were found in a right lateral shear zone. Since the Philippine Fault is a left-lateral shear zone, the counterclockwise rotation is expected. Also in accordance with Luyendyk's model, note the right-lateral offset on one of the northeast-southwest trending faults on Biliran Island. Thus the rotation of the older samples appears to be associated with the collisional rotation of the Philippines after its impact with the Palawan terrane. The rotation of the younger samples is associated with movement along the Philippine Fault. Poor age constraints for site JL-9 make interpretation of the clockwise rotation of this site impossible at this time. It must also be noted that incongruous inclination values for site JL-56, seen in the processed data (Table 3), eliminated this site from analysis in this study.

We are currently having the samples dated using K-Ar dating methods in order to better constrain the time period in which these rotations could have occurred. This would enable us to also make an estimate of initiation of movement along the

Philippine Fault. Land-Sat photos and updated geologic maps of Leyte would aid in further constraining the model used to predict rotation in the fault regime.

## CONCLUSION

The six sample sites appear to have been properly demagnetized as indicated by the results of the  $J/J_0$  as a function of demagnetizing field strength graph (Fig. 10) and of the Zijderfeld plot (Fig. 11). Sites JL-71 and JB-37 which contain samples of rock older than 20 my are rotated clockwise. This clockwise rotation is predicted by the collision of the Palawan continental terrane with the Philippine Archipelago. Sites JB-17, JB-3, and possibly JL-26 show counterclockwise rotation which indicates fault-generated rotations in the left-lateral shear zone of the Philippine Fault. The rotation of JL-9 could not be constrained at this time due to the unavailability of accurate age data. Constraining the timing of the rotations was a problem throughout the study area because the samples themselves have not been dated by the K-Ar method, and ages do not already exist for the geologic units from which the samples were taken.

## ACKNOWLEDGEMENTS

I would like to thank Robert McCabe, my faculty advisor, for giving me the opportunity to do this project. Many thanks to Jay Cole for his help and for his field work which made this report possible. Finally, my sincere appreciation to Kevin Looff for his help and support.

## REFERENCES

- Aquino, R.F., et.al., Semi-Detailed Geology of the Bato-Lunas and Vicinity, Burauen Geothermal Project, Leyte, Philippine National Oil Corp. Unpublished Report, 72 pg., 1983.
- Bayrante, L.F., The Geology of Burauen Geothermal Project, Leyte, Central Philippines, Philippine National Oil Corp. Unpublished Report, 127 pg., 1981.
- Beck, M.E., Discordant paleomagnetic pole positions as evidence of regional shear in the western cordillera of North America, *Am. Jour. Sci.*, 276, 694-712, 1976.
- Espiritu, D.D., Geology of Biliran Island, Leyte (Report No. 2), Philippine National Oil Corp. Unpublished Report, 42 pg., 1983.
- Luyendyk, B.P., M.J. Kamerling, and R. Terres, Geometric model for Neogene crustal rotations in southern California, *Geol. Soc. Am. Bull.*, 91, 211-217, 1980.
- McCabe, R., J. Almasco, W. Diegor, Geologic and paleomagnetic evidence for a possible Miocene collision in western Panay, central Philippines, *Geology*, 10, 325-329, 1982.
- McCabe, R., J.N. Almasco, G. Yumul, Terranes of the Central Philippines, Texas A & M Geodynamics Program Contribution Number 47, 421-435, 1985.

**Appendix**  
**Stratigraphic Columns**



LITHOLOGY	ROCK TYPE	THICKNESS (m.)	DESCRIPTION	AGE
	Alluvium (Qal)	?	Unconsolidated sand, gravel, beach sand, stream and sinter deposits.	Recent
	Bato Andesite (Qba)	400	Fresh hornblende andesite, tuffaceous volcanics with euhedral hornblende crystals.	QUATERNARY Pleistocene
	Parasanon Sedimentary Deposits (Psd)	5	Isolated clastics composed of fossiliferous siltstone, mudstone, calcisiltite and conglomerates with dacitic pumice and andesite clasts.	
	Tallsayan Volcanics (Tv)	300	Dacitic (silicic) hornblende andesite flows, andesitic/silicic flow breccia, agglomerate, pyroclastics, with occasional andesite tuff.	TERTIARY Miocene to Pliocene
	Marabong Volcanic Complex (Mvc)	300	Predominantly basaltic andesite, flow breccia, intercalation of agglomerate and lava flow with occasional tuff.	
	Calanipawan Limestone (Cl)	10	Coralline limestone with interstitial micrite containing bioclasts of amphistegina, echinoids and ostracods.	
NON CONFORMITY				
	Bito Ultramafic (Bu)	?	Highly serpentized and shattered peridotite found along major fault. Also encountered around Lake Bito.	PRE-TERTIARY ?

Fig. 7 PROPOSED TENTATIVE STRATIGRAPHIC COLUMN

**BURAUEN GEOTHERMAL PROSPECT**  
**TENTATIVE STRATIGRAPHIC COLUMN**

STRATIGRAPHIC COLUMN	ROCK UNITS	LITHOLOGY	THICKNESS (M)	PROB AGE
	RECENT DEPOSITS (Oai)	Alluvium, beach sand, spring & fluvialite deposits	10 M	RECENT
	LOCAL UNCONFORMITY			
	MAHAGNAO VOLCANICS (Omv)	Hb rich andesite, dacite lavas & pyroclastics	UNKNOWN	QUATERNARY
	LOBI VOLCANICS (Olv)	Px andesite lavas, tuffs & minor tuff breccias	UNKNOWN	
	PLUG DOMES (Osd)	Bio-bearing pyroxene hornblende andesite	240	
	BURAUEN PYROCLASTICS (Bpd)	Volcanic piedmont deposits andesite tephrae & debris	~300	
	DAGUITAN TUFF (Dt)	Hb-dacitic sandy tuff along Daguitan & Marabong	80	PLIOCENE PLEISTOCENE
	ALBUERA FORMATION (Af)	Tuffaceous ss conglomerate calcarenite, mudstone, reefal limestone & calcisiltite	250	
	LEYTE CENTRAL FORMATION (Lcf)	Volcanic breccia, agglomerate andesites, pyroclastics intruded by basaltic andesites dykes & sills	~700	
	NON CONFORMITY			
	ALBUERA DIORITE (Ad)	Bio-diorite encountered in areas near Albuera	UNKNOWN	MIOCENE
	BURAUEN VOLCANICS (Mbv)	Hb-andesite-oxy-hb andesite 2-px and., augite basalt & intercalated pyroclastics	~1000	
	LEYTE ULTRAMAFIC COMPLEX (Luc)	Calcified serpentized peridotite along fault zones & pyroxene rich ultrabasic	UNKNOWN	LATE-CRETACEOUS
	BASEMENT (?)			

**FIG. 6 TENTATIVE STRATIGRAPHIC COLUMN**

NOTE: DRAWN NOT TO SCALE

LFB - 1/22/62  
 Drawn by: CAA

STRATIGRAPHIC COLUMN	ROCK TYPE	DESCRIPTION	AGE
	OAL ALLUVIUM	ALLUVIUM & TALUS DEPOSIT	RECENT PLEISTOCENE
	VILLA VICENTA LS.	REEFAL LS.	PLEISTOCENE
	SAYAO HB DACITE & ANDESITE	LIGHT COLORED HB DACITE & PORPHYRITIC ANDESITE	↑
	BILIRAN VOLCANICS	COMPOSITE VOLCANO MADE UP OF BASALT & ANDESITE FLOWS & TUFF	
	KANDAKO BASALT	FINE-GRAINED BLACK BASALT	
	ASLUMAN VOLCANICS	VESICULAR, DARK COLORED ANDESITE	
	PANAMA O ANDESITE	FINE-GRAINED PYROXENE ANDESITE	
	CATMON PX ANDESITE	FINE & COARSE GRAINED PYROXENE LAVAS	↓
	OLDER VOLCANICS ?	PROBABLY ANDESITE & BASALT LAVAS	
	SEDIMENTARY BASEMENT	CLASTICS & CARBONATES	MIOCENE- PLIOCENE
	BASEMENT COMPLEX	METAVOLCANICS & ULTRAMAFICS	PRE-MIOCENE

NOT DRAWN TO SCALE

BILIRAN IS.

TENTATIVE STRATIGRAPHIC COLUMN  
DDE / DBL

PNOC-ENERGY DEVELOPMENT CORPORATION  
GEO THERMAL DIVISION  
MERRITT ROAD FORT BONIFACIO METRO MANILA

FIG. 4 TENTATIVE STRATIGRAPHIC COLUMN OF BILIRAN